The two-dimensional turbulent wall-jet

By W. H. SCHWARZ AND W. P. COSART
Department of Chemical Engineering, Stanford University, Palo Alto, California

(Received 1 November, 1960)

With the aid of a hot-wire anemometer, the mean velocity distribution of the incompressible, turbulent, plane wall-jet has been examined in some detail. As previously reported, this fully developed boundary layer belongs to the class of self-preserving flows. Over the entire range of experimental conditions, a single velocity scale ($\overline{U}_m$) and a single length scale (δ) seem to correlate all the velocity data. Further, it is shown theoretically that δ must vary as x, and $\overline{U}_m$ must vary as x^a over this range. The exponent a has been empirically determined as $-0{\cdot}555$. Values of the Reynolds shear stress, which are proportional to $\overline{uv}$, the Boussinesq exchange coefficient ϵ, and the shear stress at the wall have been evaluated. The Reynolds number based on the maximum velocity and the thickness of the boundary layer varied from 22,000 to 106,000.

1. Introduction

The wall-jet is described as a jet of fluid which impinges onto a wall at an angle from 0 to 90 degrees. The region of interest is the fully developed boundary layer which occurs after the stagnation flow and the turbulent transition regions, and has both a solid boundary and a free boundary of the same fluid as the jet. The name wall-jet seems to have been ascribed by Glauert (1956), although the terms partially open jet, surface jet, and submerged jet have been used by Förthmann (1934), Zerbe & Selna (1946) and Poreth & Cermak (1959).

Since the boundary conditions on the surface jet are such that the velocity at the wall and also outside the boundary layer are zero, the velocity profile must have a maximum. Further, this flow is of the self-preserving class of shear flows such as jets, wakes, and free-mixing layers. The free and solid boundaries generate considerable interest, since the flow will have both a jet-like property and also be influenced by the wall. A sketch of the tangential wall-jet is shown in figure 1, which includes a fully developed profile.

The earliest known work on the plane wall-jet was done by Förthmann (1934), apparently to complement his investigation of the plane free jet and partially expanding jet. Förthmann observed the self-preserving nature of the wall-jet, and that the boundary-layer thickness varied linearly with x and the maximum velocity varied inversely as the half power of x. Further, he determined from the data that the velocity in the inner layer varied as the one-seventh power of the distance from the wall.

Glauert (1956) has examined theoretically the similarity problem of the laminar and turbulent, radial and plane wall-jets. The velocity distribution of

the turbulent radial wall-jet and the variation of velocity and length scales with downstream position has been measured by Bakke (1957). He found that the velocity scale varied as a power of x with exponent $-1{\cdot}12 \pm 0{\cdot}03$ and the length scale as $0{\cdot}94 \pm 0{\cdot}02$. The velocity profiles showed a self-preserving character in both the inner and outer layers.

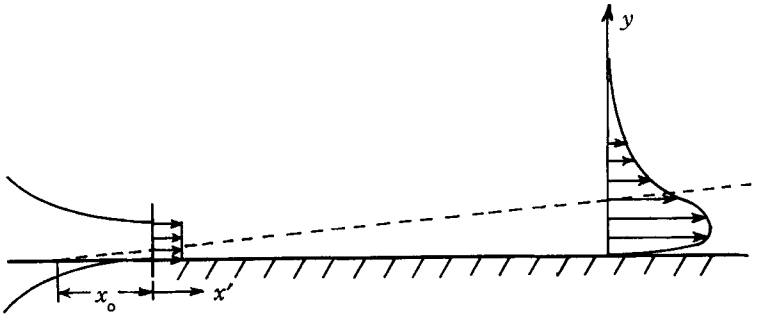

FIGURE 1. Tangential wall-jet.

The measurement of wall shear stress in a tangential jet was done by Sigalla (1958*b*). Data were correlated in a manner analogous to that of a turbulent boundary layer on a flat plate. The boundary-layer thickness was found experimentally to vary linearly, making an angle of 3·7 degrees with the plate and passing approximately through the centre of the outlet nozzle of the jet. Further, it was found that the velocity scale varied as a power of x with an exponent of minus one-half.

2. Theoretical development

The equations of motion for a steady, plane, turbulent, incompressible flow with constant physical properties and negligible energy dissipation may be written as

$$\overline{U}\frac{\partial \overline{U}}{\partial x}+\overline{V}\frac{\partial \overline{U}}{\partial y}=-\frac{1}{\rho}\frac{\partial \overline{p}}{\partial x}+\frac{\partial}{\partial x}\left[\nu\frac{\partial \overline{U}}{\partial x}-\overline{u^2}\right]+\frac{\partial}{\partial y}\left[\nu\frac{\partial \overline{U}}{\partial y}-\overline{uv}\right], \tag{1}$$

$$\overline{U}\frac{\partial \overline{V}}{\partial x}+\overline{V}\frac{\partial \overline{V}}{\partial y}=-\frac{1}{\rho}\frac{\partial \overline{p}}{\partial y}+\frac{\partial}{\partial x}\left[\nu\frac{\partial \overline{V}}{\partial x}-\overline{uv}\right]+\frac{\partial}{\partial y}\left[\nu\frac{\partial \overline{V}}{\partial y}-\overline{v^2}\right], \tag{2}$$

$$0=\frac{\partial \overline{uw}}{\partial x}+\frac{\partial \overline{vw}}{\partial y}. \tag{3}$$

The continuity equation is written

$$\frac{\partial \overline{U}}{\partial x}+\frac{\partial \overline{V}}{\partial y}=0. \tag{4}$$

When the boundary-layer approximations are applied to (1), we obtain

$$\overline{U}\frac{\partial \overline{U}}{\partial x}+\overline{V}\frac{\partial \overline{U}}{\partial y}+\frac{\partial}{\partial x}(\overline{u^2}-\overline{v^2})+\frac{\partial \overline{uv}}{\partial y}=\nu\frac{\partial^2 \overline{U}}{\partial y^2}. \tag{5}$$

Then the following functions may be defined

$$\overline{U}=U_0 f(\eta),\quad \overline{u^2}=U_0^2 g_1(\eta),\quad \overline{v^2}=U_0^2 g_2(\eta),\quad \overline{uv}=U_0^2 g_{12}(\eta),\quad \eta=y/\delta. \tag{6}$$

If (6) are substituted into (5), with suitable rearrangement, the following form is obtained

$$\underset{(a)}{\frac{\delta}{U_0}\frac{\partial U_0}{dx}f(\eta)^2}-\underset{(b)}{\frac{1}{U_0}\frac{d(U_0\delta)}{dx}\frac{df(\eta)}{d\eta}\int_0^\eta f(\eta)\,d\eta}+\underset{(c)}{\frac{2\delta}{U_0}\frac{dU_0}{dx}g_1(\eta)}$$

$$-\underset{(d)}{\frac{d\delta}{dx}\eta\frac{dg_1(\eta)}{d\eta}}+\underset{(e)}{\frac{d\delta}{dx}\eta\frac{dg_2(\eta)}{d\eta}}-\underset{(f)}{2g_2(\eta)\frac{\delta}{U_0}\frac{dU_0}{dx}}+\underset{(g)}{\frac{dg_{12}(\eta)}{d\eta}}=\underset{(h)}{\frac{\nu}{U_0\delta}\frac{d^2f(\eta)}{d\eta^2}}. \quad (7)$$

If the flow is self-preserving, the functions $f(\eta)$, $g_1(\eta)$, $g_{12}(\eta)$, and $g_2(\eta)$ are independent of x, and hence the solution of (7) requires that the coefficients of the universal functions be either non-zero constants or zero. For a non-trivial solution, consider the ratios to be non-zero. The non-repetitive coefficients are

$$\frac{\delta}{U_0}\frac{dU_0}{dx}, \quad \frac{d\delta}{dx} \quad \text{and} \quad \frac{\nu}{U_0\delta}. \quad (8)$$

Each of these coefficients must be equal to a constant, hence

$$\delta = C_2 x \quad \text{and} \quad U_0 = C_0 x^{-1}. \quad (9,10)$$

This result uses the viscous shear stress term (h).

Now it is a well-known fact that in any turbulent flow, the viscous stress is small compared to the turbulent shear stress (term (g)), except very close to a wall. In the present investigation, the viscous shear stress was only 3 % of the turbulent shear stress even at 0·2 mm from the wall, which was the closest point at which the experimental equipment could be used. It seems reasonable therefore to neglect term (h). Then the only non-repetitive constant coefficients are

$$\frac{d\delta}{dx} \quad \text{and} \quad \frac{\delta}{U_0}\frac{dU_0}{dx}. \quad (11)$$

Solving these two equations gives

$$\delta = C_2 \quad U_0 = C_1 x^a, \quad (12)$$

or that the length scale varies linearly with x and the velocity scale varies as a power of the downstream direction. From the above analysis, it is seen that the flow is unlikely to have the same self-preserving character over the entire width of the boundary layer. Very near the wall, the viscous terms will dominate and the velocity scaling factor will have a different x-variation from that of the outer flow. However, for the regions of the flow that were examined, the viscous term was negligible.

If (5) is integrated with respect to y from 0 to ∞, and (4) is used, we find that

$$\frac{\tau_w}{\rho} = -\int_0^\infty \frac{\partial}{\partial x}(\overline{U}^2+\overline{u^2}-\overline{v^2})\,dy. \quad (13)$$

Since $\overline{u^2}-\overline{v^2} \ll \overline{U}^2$, and making use of (6), (13) becomes

$$\frac{\tau_w}{\rho} = -\left(2\delta U_0\frac{dU_0}{dx}+U_0^2\frac{d\delta}{dx}\right)\int_0^\infty f^2(\eta)\,d\eta. \quad (14)$$

Then, with the forms of the x-variation of δ and U_0, this may be written

$$\frac{\tau_w}{\rho} = -C_1^2 C_2 x^{2a}(2a+1)\int_0^\infty f^2(\eta)\,d\eta. \tag{15}$$

A skin friction coefficient may be defined by

$$C_f = \frac{\tau_w}{\frac{1}{2}\rho \overline{U}_m^2}. \tag{16}$$

Then

$$C_f = -2C_2(2a+1)\int_0^\infty f^2(\eta)\,d\eta. \tag{17}$$

From (15), it is apparent that the exponent of the x-variation of the velocity scale must be less than $-\frac{1}{2}$. If it were not, the shear stress on the wall would be either zero or negative, which are both impossible.

	Laminar		Turbulent	
	U_0	δ	U_0	δ
Plane jet	$x^{-\frac{1}{2}}$	$x^{\frac{1}{2}}$	$x^{-\frac{1}{2}}$	x
Plane wall-jet	$x^{-\frac{1}{2}}$	$x^{\frac{1}{2}}$	$x^{-0.555}$*	x
Circular jet	x^{-1}	x	x^{-1}	x
Circular wall-jet	$x^{-\frac{3}{4}}$	$x^{\frac{1}{4}}$	$x^{-1.12}$	$x^{0.94}$†
Flat plate ($dp/dx = 0$)	x^0	$x^{\frac{1}{2}}$	x^0	$x^{\frac{4}{5}}$

* Data of Cosart (1960). † Data of Bakke (1957).

TABLE 1

From the equations of motion, a relationship between the exponents of the x-variation of the length and velocity scales has been obtained. However, a second relation is necessary if a is to be determined uniquely. For a free jet flow, this relation is obtained from the constancy of the flux of momentum. In the Blasius problem, the velocity scale varies as the free stream velocity or is a constant. Similarly, when the potential flow over a solid surface varies as x^m, then the velocity scale will have the same variation. Glauert (1956) has succeeded in obtaining a second relation for the laminar wall-jet by noting that the 'flux of exterior momentum flux' is constant. This approach is not applicable to the turbulent wall-jet. The results of various similar flows are compared in table 1.

Now (7) may be rearranged to give (neglecting the viscous term)

$$g_{12}(\eta) = \left[2\frac{\delta}{U_0}\frac{dU_0}{dx} + \frac{d\delta}{dx}\right]\int_\eta^\infty f^2(\eta)\,d\eta + \left[\frac{\delta}{U_0}\frac{dU_0}{dx} + \frac{d\delta}{dx}\right] f(\eta)\int_0^\eta f(\eta)\,d\eta. \tag{18}$$

Then substituting (12) into (18), we obtain

$$g_{12}(\eta) = C_2(2a+1)\int_\eta^\infty f^2(\eta)\,d\eta + C_2(1+a) f(\eta)\int_0^\eta f(\eta)\,d\eta. \tag{19}$$

The function $g_{12}(\eta)$ is the universal turbulent shear-stress function.

The Boussinesq exchange coefficient may be defined by

$$\epsilon \frac{\partial \overline{U}}{\partial y} = -\overline{uv}. \tag{20}$$

Therefore, from (6) and defining $\tilde{\epsilon}$ as $\epsilon/U_0\delta$, we have that

$$\tilde{\epsilon} = -g_{12}(\eta)/f'(\eta). \tag{21}$$

3. Experimental method

The wind-tunnel facility used in the investigation consisted of a variable-speed blower, a diffuser section, a plenum chamber or calming section, a contraction and the flat plate. The blower was driven by a variable-speed DC motor and produced a range of velocities at the outlet of the contraction from about 0 to 85 ft./sec. The diffuser and calming section contained a number of screens to reduce turbulence, produce a uniform velocity distribution, and prevent separation in the diffuser. The contraction had an area ratio of 24 to 1 with a 24×1 in. outlet, and further served to produce a uniform and low turbulence velocity distribution at the outlet. The contraction was smoothly joined to a flat plate so that the flow was tangential to the plate. The plate had a smooth aluminium sheet attached to it and was approximately 6 ft. long. Side-boards were attached to the plate to prevent the flow from spilling over the edge and thus interfering with the two-dimensionality of the flow.

All mean velocities of the wall-jet boundary layer were measured with a hot-wire anemometer. The wire element was Wollaston drawn platinum, 0·00025 in. in diameter. The actual position of the wire from the plate was determined with a cathetometer, sensitive to within $\frac{1}{20}$ mm. The wire was easily visible with the telescope and cross-hairs. The actual distance of the wire from the plate was determined by several observations of the wire and its reflected image. The downstream position of the wire from the nozzles was measured with a common pocket tape to within $\frac{1}{8}$ in.

4. Results

A series of velocity tranverses were taken with nozzle speeds of 27, 40, 60, and 83 ft./sec over a range of distance downstream of the outlet from 1·5 to 5·5 ft. A typical set of data is shown in figure 2. The curve drawn through the points is the universal curve which is explained below. For the set of runs, values of the maximum velocity and boundary-layer thickness are listed in table 2.

All the mean velocity data were plotted together in dimensionless form and a single curve drawn through the points. This universal curve is shown in figure 3. From figure 2, typical departures of the data from the universal curve may be seen.

The variation of the boundary-layer thickness with distance has been previously shown to be proportional to the distance from the virtual origin and is of the form given by (12). This equation may be written as

$$\delta = C_2(x' + x_0), \tag{22}$$

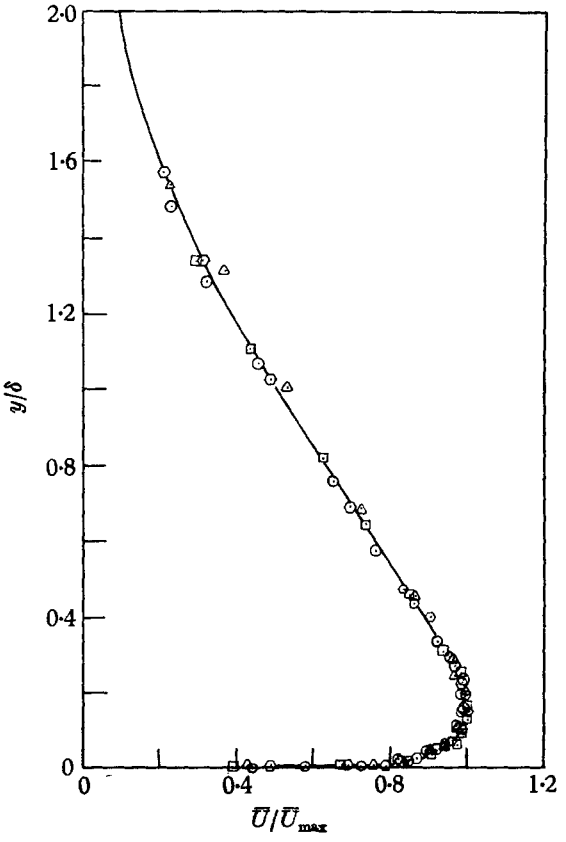

FIGURE 2. Velocity profile: the data points were taken with an outlet nozzle velocity of 83 ft./sec and at four downstream positions. ⊙, $x' = 2{\cdot}0$ ft.; ⊙, $x' = 2{\cdot}5$ ft.; △, $x' = 3{\cdot}0$ ft.; ⊡, $x' = 3{\cdot}5$ ft.

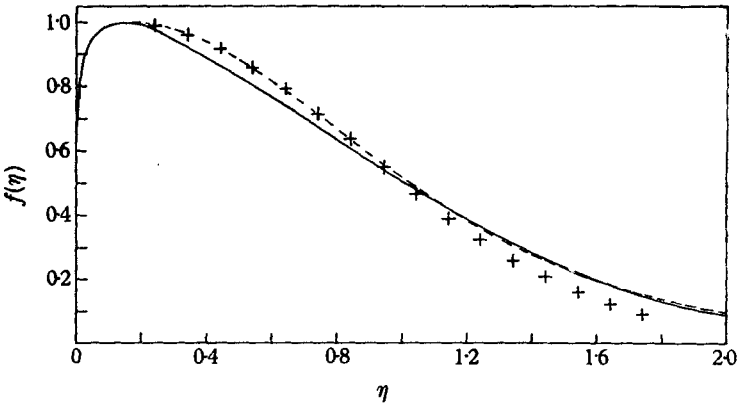

FIGURE 3. Universal velocity profile: ——, experimental data; – – – –, $\text{sech}^2(\eta - 0{\cdot}14)$; +, $\exp[0{\cdot}937(\eta - 0{\cdot}14)^2]$.

where x_0 is the distance from the outlet of the wind tunnel to the point where the turbulence is assumed to originate (the virtual origin). Further, the variation of the maximum velocity with downstream position may be written as

$$\overline{U}_m = C_1(x' + x_0)^a. \tag{23}$$

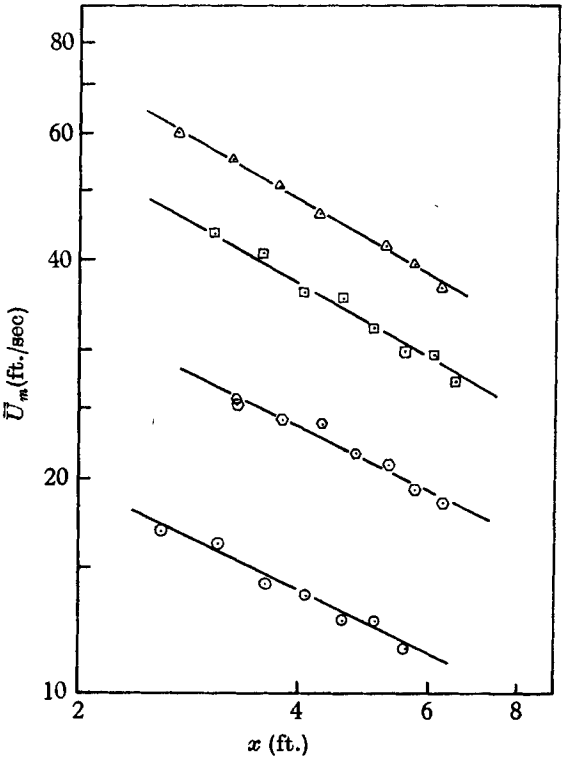

FIGURE 4. Variation of velocity scale: ⊙, $V_0 = 27$ ft./sec.; ⊙, $V_0 = 40$ ft./sec; ⊡, $V_0 = 60$ ft./sec; △, $V_0 = 83$ ft./sec.

V_0 (ft./sec)	x_0 (ft.)	C_1 (ft.$^{1-a}$/sec)	$C_2 = h(R_0)$	a	R_0	$f_1(R_0)$
27	0·60	36·4	0·0851	$-0·50 \pm 0·09$	13,510	4·67
40	1·297	46·8	0·0694	$-0·50 \pm 0·09$	20,100	4·06
60	1·077	88·7	0·0561	$-0·62 \pm 0·08$	30,000	6·90
83	0·748	113·3	0·0607	$-0·60 \pm 0·04$	41,600	5·95
Average value	0·931	—	0·06782	$-0·555$	—	5·395

TABLE 2

Values for the virtual origin x_0 and the constant C_2 were determined from (22) for each outlet velocity. Then the exponent a and the constant C_1 were obtained from (23) and are given in table 2. These values were obtained by means of a least squares fit of the experimental data and the 95 % confidence intervals were evaluated. A plot of $\overline{U}_m$ versus x is shown in figure 4, for the various outlet velocities.

The inner layer

Some of the velocities measured in the inner layer are presented in figure 5. The plot has logarithmic scales and shows $\overline{U}/U_m$ versus y/δ. It is readily seen that over the whole range of experimental conditions, the data are correlated with the velocity scale $\overline{U}_m$ and the length scale δ. Near the wall, scatter of data was appreciable. This is due to the extremely small distance from the wall (of the order of 0·2 mm). However, from this plot and also a linear plot (not shown), there does not appear to be any systematic variation within the data. It is therefore concluded that the same velocity scale and length scale applies to the whole boundary layer except very close to the wall ($\eta < 0{\cdot}005$).

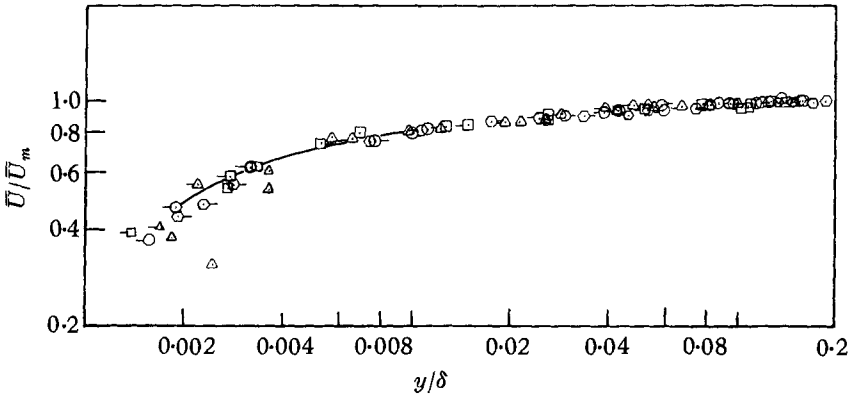

FIGURE 5. The inner layer: the data points shown span the entire outlet velocity range and downstream positions.

V_0	(ft./sec)	x' (ft.)	V_0	(ft./sec)	x' (ft.)
⊙	26·0	2·0	⊡	60·7	5·0
◇	26·2	4·5	△	60·3	5·5
△	34·9	2·5	⊙	83·4	4·5
□	40·0	2·5	⊡	83·1	5·0
⊙	40·2	3·0	△	86·1	5·5
◇	40·2	4·5			

The only previous measurements of the velocity distribution in the inner layer of the two-dimensional wall-jet were obtained by Förthmann (1934). He concluded that the velocity profile varied as the classic one-seventh power of the distance from the wall. The present results show the exponent to be $1/(14 \pm 1)$. Nearly 90% of the inner layer follows this relationship, i.e. for η lying between approximately 0·01 and 0·13. The curve deviates from this relation near the maximum and near the wall.

The one-seventh power law adopted by Förthmann (1934), Glauert (1956), and Sigalla (1958*a*) seems to have been obtained by considering the inner layer of the wall jet to be analogous to the turbulent boundary layer. As a first-order engineering approximation this analogy may be used, if the proper adjustments are made. However, there are certain important dissimilarities between the turbulent boundary layer and the inner layer of the wall-jet. The most important

difference is that of the intermittent nature of the outer part of the turbulent boundary layer. For at least 60% of the thickness of the turbulent boundary layer the flow is characterized by alternate periods of turbulent and non-turbulent flow. Another point of difference lies in the modification of the structure of the inner layer of the wall-jet by the turbulence in the outer layer. Further, the skin-friction coefficient of a turbulent boundary layer varies in a manner different from that of the wall-jet. These factors may lead to serious discrepancies for certain conditions, if the inner layer of the wall-jet is considered to be completely analogous to the turbulent boundary layer.

Dimensional analysis

Since the maximum velocity is a function of the downstream distance from the virtual origin, the outlet velocity, the viscosity and density of the fluid and the width of the nozzle, dimensional analysis shows that

$$\bar{U}_m/V_0 = f(x/d_0, V_0 d_0/\nu). \tag{24}$$

Using (12), (24) may be rewritten as

$$\bar{U}_m/V_0 = (x/d_0)^a f_1(R_0). \tag{25}$$

Hence comparing (12) and (25), it is found that

$$f_1(R_0) = C_1 d_0^a/V_0. \tag{26}$$

The values of $f_1(R_0)$ are listed in table 2 for the several outlet velocities. There is no apparent functional variation with Reynolds number (R_0) of either the virtual origin or the function $f_1(R_0)$. If the average values of $f_1(R_0)$, a, and x_0 are determined for the four outlet conditions, (25) may be written as

$$\bar{U}_m/V_0 = 5{\cdot}395(x'/d_0 + 11{\cdot}2)^{-0{\cdot}555}. \tag{27}$$

Similarly, the boundary-layer thickness is a function of the outlet velocity of the nozzle, the distance from the virtual origin, the viscosity and density of the fluid, and the width of the nozzle. Hence, the dimensionless equation is written

$$\delta/d_0 = h(x/d_0, R_0). \tag{28}$$

From the concept of self-preservation, (28) may be rewritten as

$$\delta/d_0 = (x/d_0)\, h_1(R_0). \tag{29}$$

Therefore comparing (12) and (29),

$$C_2 = h_1(R_0). \tag{30}$$

From the values of C_2 listed in table 2, there does not seem to be any systematic change in $h_1(R_0)$ as the outlet Reynolds number is varied. The average of $h_1(R_0)$ is found to be 0·0678, and the equation (28) is written

$$\delta/d_0 = 0{\cdot}0678(x'/d_0 + 11{\cdot}2). \tag{31}$$

Equations (27) and (31) are approximate formulae and are dependent on the individual system. In particular, the location of the virtual origin is a function of many conditions, such as the free-stream turbulence in the jet, the wall roughness, vibration, sound, and in fact, all the variables which affect the transition

of a laminar flow to a turbulent flow. Hence, each system will have its own specific value for the virtual origin and the virtual origin may vary with the outlet Reynolds number. From these experiments, there is no determinate functional variation of the virtual origin with the outlet Reynolds number, and the average value is used.

If the outlet Reynolds number differs significantly from the range 13,000 to 40,000, the functions $f_1(R_0)$ and $h_1(R_0)$ may change. However these functions at most vary slowly with the outlet Reynolds number.

The angle between the locus of points of the boundary-layer thickness and the plate was computed from (31) and found to be 3·8°. This value may be compared to that of Sigalla (1958*a*) which was 3·7°. Since Sigalla's measurements were in the range of R_0 lying between 20,000 and 50,000, this is not surprising.

Turbulent shear stress

The Reynolds shear stress may be written as

$$\tau_t = -\rho\,\overline{uv}. \tag{32}$$

Also, using (19), (30), the average values of $h_1(R_0)$ and table 2, the dimensionless correlation function becomes

$$g_{12}(\eta) = -0{\cdot}007458\int_{\eta}^{\infty} f^2(\eta)\,d\eta + 0{\cdot}03017 f(\eta)\int_0^{\eta} f(\eta)\,d\eta. \tag{33}$$

This function has been evaluated graphically utilizing the universal velocity function and is shown in figures 6 and 7. Since the contribution to the total shear stress from the viscous terms is very much smaller than the turbulent shear stress (of the order of 3 % very close to the wall), the total shear stress at any η is very closely approximated by (32). A dimensionless shear stress is then defined as

$$c_{f,\eta} = \tau_t/\tfrac{1}{2}\rho\overline{U}_m^2 \tag{34}$$

and hence

$$c_{f,\eta} = -2g_{12}(\eta). \tag{35}$$

From figure 6, it is seen that the correlation function is not equal to zero at η_m which corresponds to the point where the maximum velocity occurs. The two-layer theory becomes suspect since the correlation function $\overline{uv}$ is zero at the outer edge of a turbulent boundary layer and at the centre-line of a symmetrical free jet. These two conditions are not met in the turbulent wall-jet. Further, the shear stress at the point where the maximum velocity occurs is non-zero, at least to the accuracy of the present data. This phenomenon is a consequence of the asymmetrical shape of the velocity distribution.

The Boussinesq exchange coefficient

The dimensionless exchange coefficient or eddy diffusivity has been previously defined in (21). The experimental determination of this quantity involved the graphical differentiation of the universal velocity profile. Also, as previously mentioned, the dimensionless correlation function $g_{12}(\eta)$ was obtained by graphical integration. These numerical techniques, especially the evaluation of the derivative, often produce results which are moderately inaccurate, even when exceptional care is taken with the data.

Values of the exchange coefficient $\tilde{\epsilon}$, as a function of η, were evaluated as mentioned above, and the smoothed data are plotted in figures 6 and 7 for the outer and inner layers, respectively.

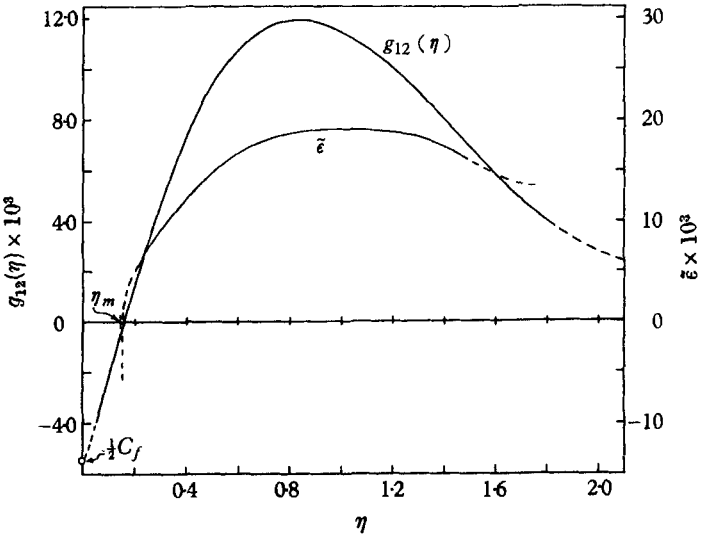

FIGURE 6. Universal correlation function and exchange coefficient.

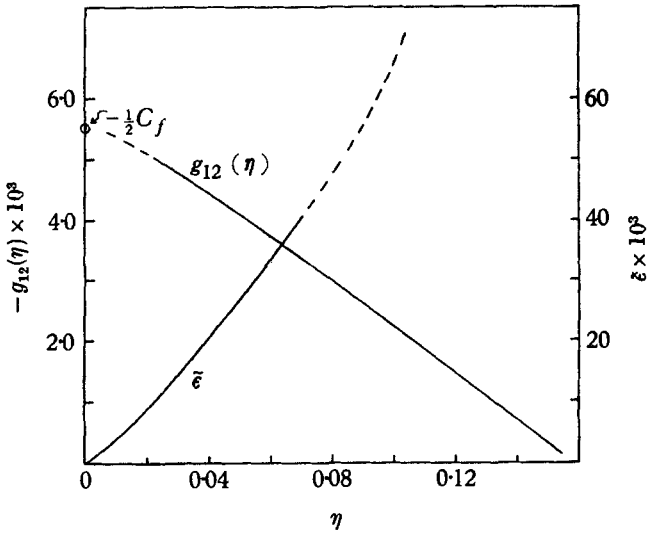

FIGURE 7. Universal correlation function and exchange coefficient for the inner layer.

In the outer layer, the eddy diffusivity shows a similar behaviour to that observed in a two-dimensional free jet. The values of the exchange coefficient are fairly constant in the middle portion and diminish toward the outer edge. However, toward the velocity maximum or where the derivative of the velocity becomes zero, the eddy diffusivity will go to infinity since a finite value is

divided by zero. Also, the eddy diffusivity will change sign near the velocity maximum since $g_{12}(\eta)$ changes sign and hence tends towards minus infinity. This obviously presents some interesting operational difficulties when the concept of an exchange coefficient is employed.

In the inner layer, the functional behaviour of the eddy diffusivity from the wall outward somewhat resembles that of a turbulent boundary layer, except that as η_m is approached, the coefficient tends toward positive infinity. In a turbulent boundary layer or a turbulent pipe flow, the $\overline{uv}$ correlation tends to zero at the outer edge and the centre line, respectively. The form of the exchange coefficient is then indeterminate However, L'Hospital's rule may be applied and it may be shown that the coefficient tends towards a constant if the velocity distribution is parabolic where the derivative goes to zero. For the wall-jet, the $\overline{uv}$ correlation is non-zero, hence the form of $\bar{\epsilon}$ will tend towards infinity.

5. Law of the wall

It has been postulated that near a smooth wall, the velocity profile of an incompressible flow is of the form

$$\overline{U}/U^* = k(yU^*/\nu), \tag{36}$$

where U^* is the friction velocity and is equal to $(\tau_w/\rho)^{\frac{1}{2}}$. Very near the wall, in the laminar sublayer, (36) has the form

$$\overline{U}/U^* = yU^*/\nu. \tag{37}$$

This is obtained from the assumption that the sublayer is so thin that the shear stress is constant across its width and hence the velocity is proportional to y, or conversely this behaviour defines the laminar sublayer.

In the outer layer of a turbulent flow, such as a pipe or boundary layer, the velocity assumes the form

$$(\overline{U}-\overline{U}_m)/U^* = j(y/\delta) \tag{38}$$

which is often called the velocity defect law. Since (36) and (38) overlap, (36) must have the form

$$\frac{\overline{U}}{U^*} = A\log\frac{yU^*}{\nu}+B \tag{39}$$

in the overlap region. The constants A and B have been given by Clauser (1956) as 5·6 and 4·9, respectively, and were obtained from the compilation of data obtained in turbulent boundary layers with and without pressure gradients and in turbulent pipe and channel flows.

The terms in (36) may be rearranged into the forms

$$\frac{\overline{U}}{U^*} = 13{\cdot}41f(\eta) = k\left(\frac{yU^*}{\nu}\right) = k(38{\cdot}5\eta x^{0{\cdot}445}V_0) \tag{40}$$

which are obtained from (15), (6) and (12), and the average values of C_1, C_2 and α. But $f(\eta)$ is a universal function of η and is independent of x and V_0. Therefore, (36) cannot represent the data as long as the universal function applies, i.e. $\overline{U}/\overline{U}_m = f(\eta)$. Now, the velocity defect law may be rewritten as

$$(\overline{U}-\overline{U}_m)/U^* = g(\eta) \tag{41}$$

and from (15) $$U^* = C_1 x^a \left\{ -C_2(2a+1) \int_0^\infty f^2(\eta)\, d\eta \right\}. \tag{42}$$

Then, defining $$C_3 = -C_2(2a+1) \int_0^\infty f^2(\eta)\, d\eta, \tag{43}$$

equation (41) may be rewritten

$$\frac{\overline{U}_m[f(\eta)-1]}{C_3 C_1 x^a} = \frac{f(\eta)-1}{C_3} = g(\eta). \tag{44}$$

Hence the velocity defect law is linearly proportional to the present similarity law used to correlate the wall-jet data.

The similarity law correlates the velocity data to the value of η of at least 0·01. If the corresponding value of yU^*/ν is estimated from equation (40), the value is 21·3 for $V_0 = 27$ ft./sec, $x = 5$ ft., and $\nu = 0{\cdot}166 \times 10^{-3}$ ft.^{2}/sec. This value lies well within the logarithmic region of (39), but (39) is not applicable since the similarity law will still correlate the data.

A 'law of the wall' may still apply to the region very near the boundary of the turbulent wall-jet; however, the constants obtained from measurements taken in turbulent boundary layers, pipe and channel flows appear to be inapplicable to the wall-jet flow. Unfortunately the present experimental technique did not allow a study of this inner inner-layer.

6. The skin-friction coefficient

The skin-friction coefficient was evaluated from (17) by graphical integration and using the average value of $h_1(R_0)$. It was found that

$$C_f = 1{\cdot}109 \times 10^{-2}. \tag{45}$$

This is the average value for the present experimental conditions and it is independent of the downstream position and at most a slowly varying function of the outlet Reynolds number, R_0.

This value is in conflict with the work of Sigalla (1958*b*) who has correlated his data in the form

$$C_f = 0{\cdot}0565\,(\overline{U}_m \delta_m/\nu)^{-\frac{1}{4}}. \tag{46}$$

Equation (46) may be rearranged to give

$$C_f = 0{\cdot}0565(R)^{-\frac{1}{4}}(\delta_m/\delta)^{-\frac{1}{4}}. \tag{47}$$

Now since $$R = \overline{U}_m \delta/\nu = C_1 C_2\, x^{a+1}/\nu, \tag{48}$$

$$C_f \propto (x^{0{\cdot}445})^{-\frac{1}{4}} = (x)^{-0{\cdot}111}. \tag{49}$$

This equation gives the variation of the skin-friction coefficient with x according to Sigalla, using the present results for the variation of the length and velocity scales. However, (45) shows that the skin-friction coefficient is constant for the present set of measurements.

In the present work, the Reynolds number of the boundary layer varied from about 22,000 to 106,000. If these extremes are substituted into (46) and δ_m/δ set equal to 0·14, C_f will vary from 0·00743 to 0·00513. These values differ from the present results by about a factor of two. However, it might be mentioned that the absolute value of the skin-friction coefficient that was experimentally

determined is dependent on the quantity $(2a+1)$. Since a is very close to $-\frac{1}{2}$, this quantity can be in error, although the above-mentioned arguments are correct.

The results of Sigalla are based on the analogy of the inner layer of a turbulent wall-jet to that of a turbulent boundary layer. Hence the skin-friction coefficient is considered to have the same functional form as that of the turbulent boundary layer, or the Blasius form. The present results do not indicate that relationship.

Further, the skin-friction coefficients obtained by Sigalla were determined by the method of Preston (1954). It has been shown by Bradshaw (1959) that the Preston tube calibration is not independent of the pressure gradient. Sigalla calibrated his device in a pipe flow, hence in a pressure gradient, and used it in the wall-jet which is without pressure gradient. It is also noted that the primary assumption of the Preston method is that the 'law of the wall' applies to all turbulent flows near a wall. In the previous discussion, it has been shown that this assumption is not true for the turbulent wall-jet.

7. The outer layer

The universal velocity distribution in the outer layer is shown in figure 3. Also shown are curves of $\mathrm{sech}^2\eta$ and $\exp[-A(\eta-\eta_m)^2]$. It is seen that a substantial part of the data is not well represented by either functional form. The close fit of the two curves to the data at the outer edge may be purely fortuitous, since no corrections for the effect of intermittency in the outer edge of the wall-jet have been applied.

The velocity distribution for the plane wall-jet has been determined theoretically by Glauert (1956) with the assumptions that the eddy diffusivity varies as $\overline{U}^6$ in the inner layer, and is a constant in the outer layer. The x-wise variation of similarity parameters was considered to be the same for both layers. For the outer layer, a solution of the equations of motion was obtained which deviated only slightly from the square of the hyperbolic secant and the deviation probably lies well within the limits of experimental error. As a matter of fact, the solution of the equations of motion of a plane, turbulent, free jet give this variation, if it is assumed that the exchange coefficient is constant across the flow. It becomes apparent then why the true velocity distribution differs from Glauert's work, by referring to figure 6. It is seen that the dimensionless exchange coefficient deviates markedly from its constant value near the maximum point.

8. Conclusions

All mean velocity data, taken over a three and one-half fold variation in the downstream dimension and a threefold range of nozzle velocities, were found to be reduced to a single universal curve with the length scale δ and the velocity scale $\overline{U}_m$. The correlation seemed to apply over the entire measured range, at least to a minimum value of η equal to 0·005. Further, it was shown with certain assumptions that the length scale must vary as x, the distance downstream from the virtual origin, and the velocity scale must vary as x^a, where a was found equal to $-0{\cdot}555$. The assumptions were that the mean velocity and the statistical

quantities $\overline{u^2}$, $\overline{v^2}$, and $\overline{uv}$ were self-preserving with the same scales, the viscous stresses were negligibly small, and the boundary-layer approximations were applicable.

Empirical expressions were developed to correlate the length and velocity scales with the outlet velocity and widths of the nozzle, and the physical properties of the fluid.

The $\overline{uv}$ correlation as a function of the distance from the wall was computed from the mean velocity data assuming that it had self-preserving characteristics. Since there is a direct relation between the correlation function and the turbulent shear stress, which is practically equivalent to the total shear stress (viscous stresses are negligible), the shear-stress distribution in the turbulent boundary layer was determined. Of interest was the non-zero value of the shear stress or correlation function at the velocity maximum, which is due to the unsymmetrical shape of the velocity distribution. As a consequence, the measured values of the exchange coefficient or eddy diffusivity exhibit peculiar behaviour at this point, since a finite quantity is divided by a quantity which tends to zero in the limit.

It is further concluded that the 'law of the wall' is not applicable to the turbulent wall-jet in the form that was obtained by experimentation in turbulent boundary layers, and turbulent pipe and channel flows. Also, the power-law representation commonly used for turbulent boundary layers to describe the mean velocity is appreciably modified in the wall-jet. Hence, present values of skin-friction coefficients differ from previous work, where the inner layer of the wall-jet was considered to be analogous to a turbulent boundary layer. The inner layer's structure is modified from that of turbulent boundary layer by the presence of the outer layer.

In the outer layer of the wall-jet and near the position of maximum velocity, there is a considerable difference in the velocity profile from that of a free jet or a mixing layer. This is caused primarily by the effect of the inner layer on the outer layer. Further, the square of the hyperbolic secant will not represent the velocity distribution since the value of the eddy viscosity is not constant across the flow, and approaches infinity at the maximum.

REFERENCES

Bakke, P. 1957 *J. Fluid Mech.* **2**, 467.

Bradshaw, P. 1959 *Aero. Res. Coun. Lond.* Rep. no. 20, 889; F.M. 2799.

Clauser, F. H. 1956 Article in *Advances in Applied Mechanics*, **3**. New York: Academic Press Inc.

Cosart, W. P. 1960 M.S. thesis, Stanford Univ., Stanford, Calif.

Förthmann, E. 1934 *Ingenieur Archiv.* **1**, trans.: 1936 *N.A.C.A.* T.M. 789.

Glauert, M. B. 1956 *J. Fluid Mech.* **1**, 625.

Poreth, M. & Cermak, J. E. 1959 *Sixth Midwestern Conference of Fluid Mechanics.* University of Texas, Austin, Texas.

Preston, J. H. 1954 *J. Roy. Aero. Soc.* **58**, 109.

Sigalla, A. 1958*a* *Aircr. Engng.* **30**, 131.

Sigalla, A. 1958*b* *J. Roy. Aero. Soc.* **62**, 873.

Zerbe, J. & Selna, J. 1946 *N.A.C.A.* T.N. 1070.